# Development of Near-Field-Enhanced High-Fill-Factor MEMS Radiator with Shared Spring

**H Nakajima, S Oh, A Ueno, K Morimoto and Y Suzuki**
Department of Mechanical Engineering, The University of Tokyo, 7-3-1 Hongo, Bunkyo-ku, Tokyo, Japan
E-mail: nakajima@mesl.t.u-tokyo.ac.jp

**Abstract.** For precise thermal control in satellites under varying internal heat dissipation and thermal boundary condition, we propose a high-fill factor MEMS radiator enhanced by the near-field effect. We have successfully fabricated a prototype with parylene shared springs and achieved a fill factor of as high as 89 %. It is found that at the ON state, the diaphragm temperature is increased from 58.0 °C to 106.4 °C, showing 144 % enhancement in the radiation heat flux.

## 1. Introduction

For precise thermal control in satellites under varying internal heat dissipation and/or irradiation of sunlight, active radiation control has become an important technical challenge [1, 2]. We previously proposed a MEMS-based active radiator that can change the emissivity by controlling the distance between the substrate and diaphragms with the electrostatic force [3]. The heat flux ratio at the ON/OFF states has been measured for their early prototype, and up to 42 % heat flux enhancement was obtained due to the increased thermal-contact conductance [4]. The fill factor (the ratio of the actual radiation area to the projection area of the device) was higher than that of convectional devices with louvers or shutters [5], but still limited to 61 %. Compared to conventional thermal control devices like bulky heat exchangers, the proposed MEMS radiator is advantageous for next-generation small-scale satellites due to its light weight and low energy consumption.

In the present study, we redesign the MEMS radiator with shared springs for significant improvement of the fill factor. In addition, we reduce the gap between the diaphragm and the substrate at the "ON" state, in order to activate the near-field thermal radiation and thus to obtain further enhancement of the heat flux ratio. We design the structural parameters of the present device based on mechanical considerations and heat transfer analyses. With the present proof-of-concept experiments, we demonstrate the heat-flux enhancement by the near-field radiation effect for the first time.

## 2. Design of the present MEMS radiator

Figure 1 shows the principle of the electrostatically-driven MEMS radiator. At the "OFF" state, the gap between the diaphragm and the substrate is as large as several micrometers, and the radiation heat flux is determined by the Stephan-Boltzmann law. At the "ON" state, on the other hand, the gap becomes smaller than the infrared wavelength responsible for the thermal radiation, so that the heat flux is enhanced by the near-field effect. Thus the near-field thermal radiation [6, 7] is expected to enhance the heat transfer from inside the satellites to the space.

Figure 2 shows the schematic of the present MEMS radiator. Thermally-durable parylene (diX-HR, KISCO) is used for the structural material for reducing parasitic heat conduction along the spring and

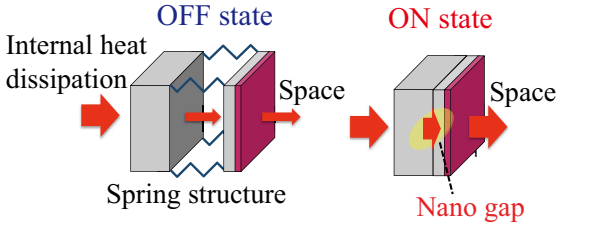


**Figure 1.** Principle of the MEMS radiator. At the "OFF" state, the thermal resistance is mainly determined by the conventional radiation. At the "ON" state, the gap between the diaphragm and the substrate becomes smaller than the nominal wavelength of thermal radiation, and thus the thermal resistance is drastically reduced due to the near-field thermal radiation effects.

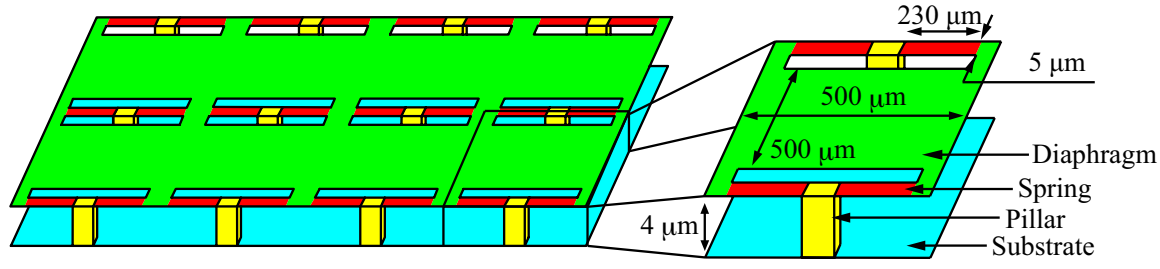


**Figure 2.** Schematic of the present MEMS radiator. Parylene is used as the structural material for reducing parasitic heat conduction along the spring and lowering the driving voltage. The parylene springs are shared among neighboring diaphragms to increase the fill factor. Compared to our previous prototype with independent diaphragms [4], the fill factor is increased from 61 % to 89 %.

for lowering the driving voltage. Parylene has low Young's modulus and low thermal conductivity, and is a proven material for the space applications [4]. The structure is basically the same as the Ueno & Suzuki's prototype [4], and the improved points are as below: 1) The parylene springs are shared among adjacent diaphragms in order to further improve the fill factor. 2) The insulating layer at the lower side of diaphragms is removed, and the thickness of the insulating layer on the substrate is decreased to 50 nm in order to reduce the gap between the substrate and the diaphragm at the ON state for the near-field effects. 3) Titanium is adopted as a top electrode material because of its low thermal conductivity, which prevents the heat conduction along the springs and improves the heat flux ratio.

The radiator performance is greatly influenced by the spring length and width. In the present design, the dimension of the springs are determined for satisfying the following three requirements: a) the driving voltage is smaller than 10 V, b) the resonance frequency is higher than 2 kHz, and c) the heat flux ratio between the ON/OFF states is maximized. For requirement a), the driving voltage is estimated from a parallel-plate capacitor model [4]. The driving voltage corresponds to the pull-in voltage, with which the diaphragm is snapped down to the bottom substrate due to the electrostatic force between the top Ti and bottom Au electrodes. For requirement b), high resonance frequency is assumed for durability against vigorous vibration during the launch of the satellite. We estimate the resonance frequency based on a spring-mass model, where the polymer springs are assumed as multi-layered cantilever beams.

For requirement c), the heat-flux ratio between the ON/OFF states is estimated from heat transfer analyses. We have performed a series of numerical simulations based on a finite volume method [8]. The amount of the heat flux from a diaphragm to the outer space is estimated for different spring length and width at the ON/OFF states. The heat balance equation for the diaphragm with the temperature $T$, the density $\rho$, the heat capacity $C_p$, and the thickness of $\Delta z$ can be expressed as:

$$\rho C_p \frac{\partial T}{\partial t} = q_x + q_y + \frac{q_{far} - q_{space} + q_{con} + q_{near}}{\Delta z}, \quad (1)$$

where the heat-flux terms on the R.H.S. of equation (1) are respectively given by:

$$q_x = \lambda \frac{d^2T}{dx^2},\ q_y = \lambda \frac{d^2T}{dy^2}: \text{Two-dimensional heat conduction in the diaphragm,} \quad (2)$$

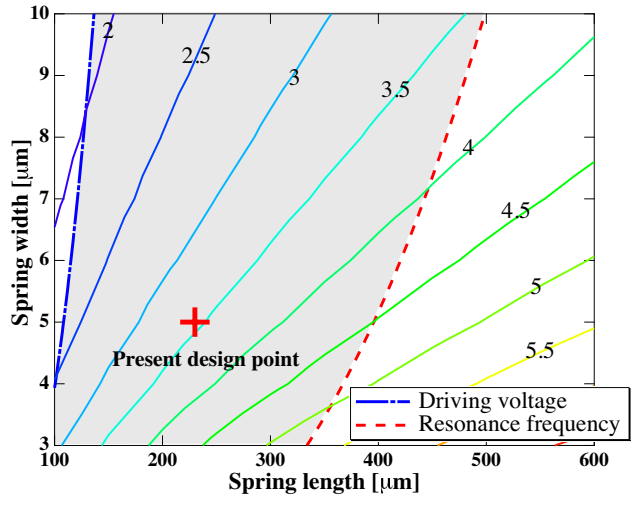


**Figure 3.** Contours of the heat flux enhancement ratio for different spring lengths and widths. The blue dashed line corresponds to the lower limit of spring length for the driving voltage < 10 V, while the red broken line sets the upper limit of the spring length for the resonant frequency > 2 kHz. By considering practical limitation of the micro fabrication process, the spring length and the width are respectively determined as 230 μm and 5 μm, which corresponds to 241 % heat flux enhancement.

$$q_{far} = \frac{\varepsilon_1 \varepsilon_2 \sigma (T_{wall}^4 - T^4)}{\varepsilon_1 + \varepsilon_2 - \varepsilon_1 \varepsilon_2} : \text{Far-field thermal radiation inside the gap,} \quad (3)$$

$$q_{space} = \varepsilon_2 \sigma (T^4 - T_{\inf}^4) : \text{Far-field thermal radiation to the space environment,} \quad (4)$$

$$q_{con} = \frac{T_{wall} - T}{R_{contact} A} : \text{Contact thermal conductance,} \quad (5)$$

$$q_{near} = \varepsilon_N \sigma (T_{wall}^4 - T^4) : \text{Near-field thermal radiation between the nano-gap.} \quad (6)$$

Here, $\lambda$ and $\sigma$ are the thermal conductivity and the Boltzmann constant, respectively. $\varepsilon_1$ and $\varepsilon_2$ are the emissivity of the substrate and the diaphragm, respectively. In the present analysis, the near-field heat flux between Ti and Au electrodes for the 100 nm gap is calculated using the previous model [6, 7], and the effective emissivity $\varepsilon_N$ due to the near-field thermal radiation is computed. $T_{wall}$ and $T_{\inf}$ denote the given temperatures at the substrate surface and for the surrounding at infinity, respectively. $R_{contact}$ and $A$ represent the contact thermal resistance [5] and the projected area of the diaphragm.

The heat flux from the substrate to the space at the OFF state is determined with the far-field radiation, the heat conduction through springs, and the heat conduction in the diaphragm. At the ON state, the near-field radiation between the nano-gap and the contact heat conduction are also involved. A second-order central differencing scheme with an Euler explicit method is employed, and the steady-state solution for the temperature distribution on the diaphragm is obtained.

Figure 3 shows the contours of the heat flux enhancement ratio for different spring lengths and widths. The substrate and surrounding temperatures are 125 °C and 27 °C respectively. The blue dashed line corresponds to the lower limit of the spring length for the driving voltage less than 10 V, while the red broken line sets the upper limit of the spring length for the resonance frequency higher than 2 kHz. Then the spring length and width should be chosen from the region between the two lines. By considering practical limitation of the MEMS-based fabrication process, in the present study, the spring length and width are determined as 230 μm and 5 μm, respectively. The fill factor of the present design is as high as 89 %. With the present geometry, 241 % heat-flux enhancement is expected.

## 3. Fabrication process

Figure 4 shows the fabrication process of the present device. Patterned Ti electrodes are covered with the parylene (diX-HR, KISCO) structures with etching holes. The whole process is summarized as: 1) Thermal oxidation of a Si wafer for electrical insulation, 2) Deposition/patterning of the bottom Cr/Au/Cr electrodes, 3) Sputtering of 50 nm-thick $SiO_2$ layer as another insulating layer. The thickness is determined in order to obtain the near-field effects. 4) Patterning of 0.2 μm-thick poly-Si as the release layer, 5) Patterning photoresist sacrificial layer, 6) Deposition of the top Ti electrode, 7) deposition of 4 μm-thick diX-HR and its patterning with etching holes as the structural layer. The etching holes are arranged on the diaphragms in order to remove the sacrificial layer smoothly. Note

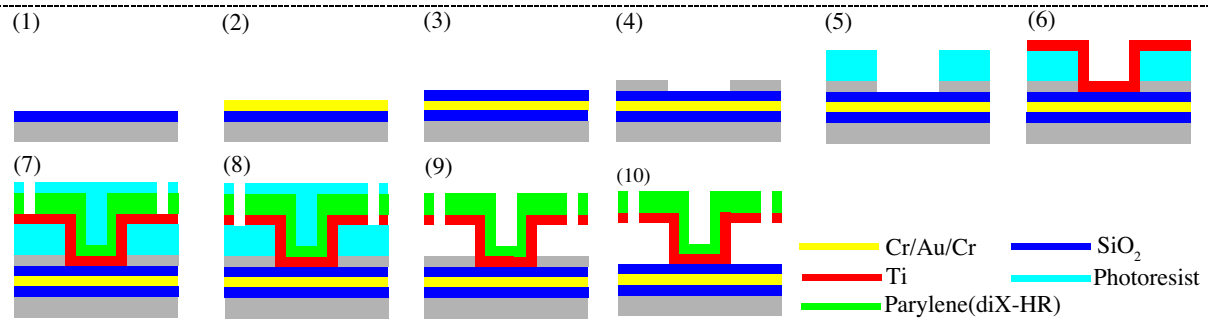


**Figure 4.** Fabrication process of the present device.

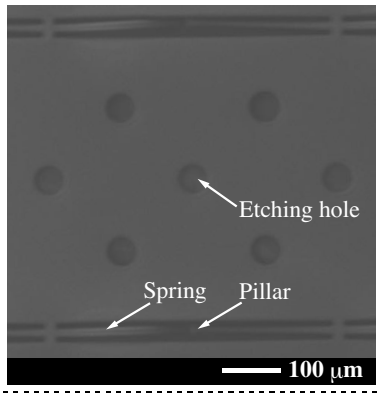


**Figure 5.** SEM image of a unit diaphragm on the present device.

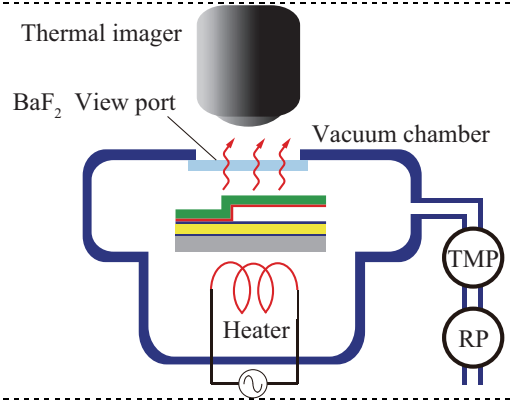


**Figure 6.** Experimental setup for thermal radiation measurements. The device is mounted on a hot chuck inside a vacuum chamber kept at 2 ~ 8 × $10^{-3}$ Pa, so that heat conduction across the gap is negligible.

that these etching holes occupy only about 5 % of the total surface area. 8) Patterning the top Ti electrode, 9) Removal of the photoresist sacrificial layer, 10) Etching of the Si sacrificial layer with $XeF_2$. Finally, as shown in Figure 5, a 22 × 22 array of the unit diaphragm is formed on a single chip.

## 4. Thermal radiation measurement

Figure 6 shows the experimental setup for thermal radiation measurements. The device is mounted on a hot chuck inside a vacuum chamber, where the chamber pressure is kept at 2 ~ 8 × $10^{-3}$ Pa. Thus the heat conduction across the gap is negligible, because the pressure is low enough to achieve the free molecular flow regime. The heater temperature is kept at 126 °C, and the surface temperature of the device is measured using a thermal imager (Apiste, FSV-1200) with a spatial resolution of ~250 μm. In the present study, the infrared-light absorption of the $BaF_2$ window of the vacuum chamber and the emissivity of the surface materials are compensated. Firstly, through a heating experiment using a sample with a black-body paint of known emissivity, the transmission rate of $BaF_2$ is estimated as 0.95. Secondly, a Si chip with a 200 nm Ti film below a 4 μm-thick parylene layer, which is the same composition as the diaphragms, was prepared, and the emissivity was measured by monitoring the surface temperature with a thermocouple. It is found that the emissivity is 0.316 at 106 °C and 0.391 at 58 °C. Somewhat large change of emissivity in a narrow temperature range is partially attributed to uncertainty of the present uncooled thermal imager at lower temperature.

Unfortunately, the present device could not be driven by the applied voltage. This is partially due to the failure of the insulating layer, but further study is needed for clarifying the reason and for achieving the active switching of the ON/OFF states. In the present study, in order to evaluate the thermal performance of the present radiator, the ON state is attained through the permanent stiction of

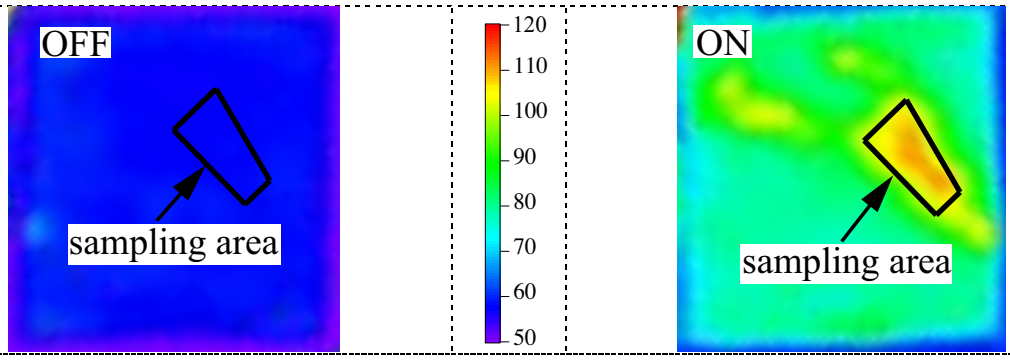


**Figure 7.** Thermal images of the present MEMS radiator for the ON/OFF states. The surface temperature is increased from 58.0 °C to 106.4 °C at the ON sate, corresponding to 144 % increase in the radiation heat flux.

the diaphragm to the substrate by applying a volatile liquid on the device.

Figure 7 shows the thermal images of the present MEMS radiator for the ON/OFF states. At the OFF state, the temperature distribution is quite uniform, and the surface temperature averaged over the sampling area (shown in the figure) is 58.0 °C. On the other hand, at the ON state, a non-uniform temperature distribution with a high-temperature area is obtained. This is attributed to the fact that the permanent stiction is achieved only at the area, which is verified by observation under microscope. The surface temperature averaged over the sampling area is increased to 106.4 °C at the ON state. This increase of the surface temperature corresponds to 144 % enhancement in the radiation heat flux. Without the near-field thermal radiation, the enhancement in the radiation heat flux is estimated in the present numerical analysis to be at most 46 %, which corresponds to the previous condition [4]. Therefore, it can be concluded that the near-field thermal radiation plays a dominant role in the drastic increase of the radiation heat flux of the present radiator. Since the numerical analysis shows 241 % heat flux enhancement, further improvement of the heat flux can be expected.

## 5. Conclusion

We have developed a high-fill-factor MEMS radiator enhanced by the near-field thermal radiation effect. We have fabricated our radiator prototype with shared springs and achieved a fill factor of as high as 89 %. It is demonstrated from proof-of-concept experiments that the surface temperature is increased from 58.0 °C at the OFF state to 106.4 °C at the ON state, which corresponds to 144 % enhancement in the radiation heat flux, showing realization of the near-field thermal radiation.

## 6. References

[1] Williams A and Palo E S 2006 *Proc. SPIE* **6221** 622108
[2] Demiryont H and Moorehead D 2009 *Sol. Energy Master. Sol. Cells* **93** 2075
[3] Ueno A and Suzuki Y 2011 *Transducers '11* (Beijing) 2654
[4] Ueno A and Suzuki Y 2014 *Appl. Phys. Lett.* **104** 093511
[5] Farrar D, Schneider W, Osiander R, Champion L J, Darrin G A, Douglas D and Swanson D T 2002 *ITHERM 2002* (San Diego) 1020
[6] Ueno A and Suzuki Y 2014 *Proc. Int. Heat Transfer Conf.* IHTC15-9636
[7] Narayanaswamy A and Chen G 2009 *Nano Lett.* **9** 2909
[8] Patankar SV 1980 *Numerical Heat Transfer and Fluid Flow* (New York: McGraw Hill)